

# Born Identity Network: Multi-way Counterfactual Map Generation to Explain a Classifier’s Decision

Kwanseok Oh<sup>1,\*</sup> Jee Seok Yoon<sup>2,\*</sup> Heung-Il Suk<sup>1,2,†</sup>

<sup>1</sup>Department of Artificial Intelligence, Korea University, Korea

<sup>2</sup>Department of Brain and Cognitive Engineering, Korea University, Korea

{ksohh, wltjr1007, hisuk} @korea.ac.kr

## Abstract

*There exists an apparent negative correlation between performance and interpretability of deep learning models. In an effort to reduce this negative correlation, we propose Born Identity Network (BIN), which is a post-hoc approach for producing multi-way counterfactual maps. A counterfactual map transforms an input sample to be classified as a target label, which is similar to how humans process knowledge through counterfactual thinking. Thus, producing a better counterfactual map may be a step towards explanation at the level of human knowledge. For example, a counterfactual map can localize hypothetical abnormalities from a normal brain image that may cause it to be diagnosed with a disease. Specifically, our proposed BIN consists of two core components: Counterfactual Map Generator and Target Attribution Network. The Counterfactual Map Generator is a variation of conditional GAN which can synthesize a counterfactual map conditioned on an arbitrary target label. The Target Attribution Network works in a complementary manner to enforce target label attribution to the synthesized map. We have validated our proposed BIN in qualitative, quantitative analysis on MNIST, 3D Shapes, and ADNI datasets, and show the comprehensibility and fidelity of our method from various ablation studies.*

## 1. Introduction

As deep learning has shown its success in various domains, there has been a growing need for interpretability and explainability in deep learning models. The black-box nature of deep learning models limits their real-world applications in fields, especially, where fairness, accountability, and transparency are essential. Moreover, from the end-user point of view, it is a crucial

\*These authors equally contributed to this work.

†Corresponding author.

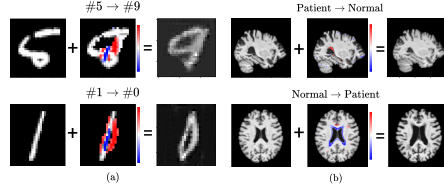


Figure 1. We propose an approach for producing counterfactual maps as a step towards counterfactual reasoning, which is a process of producing hypothetical realities given observations. For example, a counterfactual map can localize hypothetical, yet very possible, abnormalities from a brain image of a normal subject that may cause the subject to be diagnosed with a disease.

process that requires a clear understanding and explanation at the level of human knowledge. However, achieving high performance with interpretability is still an unsolved problem in the field of explainable AI (XAI) due to their apparent negative correlation [15] (*i.e.* interpretable models tend to have lower performance than black-box models).

Reducing this negative correlation in performance and interpretability has been an important agenda in the field of XAI. For example, in the early era of XAI [11], researchers have proposed various methods for discovering or identifying the regions that have the most influence on deriving the outcome of the classifier [26, 29, 30, 1, 23, 27, 28, 34]. The main objective of these early era XAI methods is to answer *why* and *how* a model has made its decision. However, recent XAI methods induce to answer the question that can offer a more fundamental explanation: “What would have caused the model to make a different decision?”. This sort of explanation is defined at the root of *counterfactual reasoning*. Counterfactual reasoning can provide an explanation at the level of human knowledge since it can explain a model’s decision in hypothetical situations, which is essentially similar to how humans process knowledge. Thus, the motivation of this paper is to show a higher-level visual explanation of a deep learning

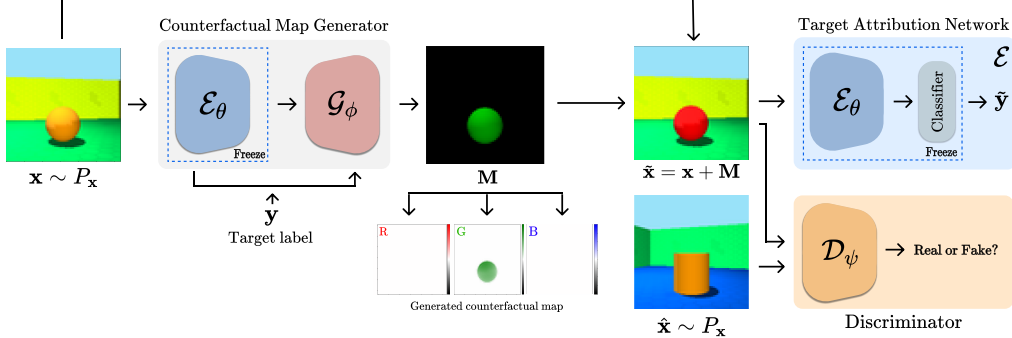


Figure 2. Schematic overview of Born Identity Network (BIN). There are two major components of BIN: Counterfactual Map Generator and Target Attribution Network. The Counterfactual Map Generator synthesized a counterfactual map conditioned on arbitrary target label, while the Target Attribution Network work towards enforcing target label attributes to the synthesized map.

model similar to that of how humans process knowledge, *i.e.*, through the means of a counterfactual map.

A *counterfactual map* is a map that can transform an input sample that was originally classified as one label to be classified as another. For example, a counterfactual map transforms a numeric image to be an image of another number (Figure 1-(a)). This counterfactual map explains what kind of structural changes are required for a numeric image to be another number. A real-world application can be of disease diagnosis (Figure 1-(b)), where a counterfactual map would describe which Region Of Interests (ROIs) may cause a normal subject to be diagnosed with a disease.

To our knowledge, most works on producing counterfactual explanations are generative models. Most notably, these works utilize Generative Adversarial Network (GAN) and its variants [12, 6, 31, 8] to synthesize a counterfactual explanation. Although these works can generate meaningful counterfactual explanations, two fundamental problems limit their application in the real world. First, generative models are a typical example of models that experience the aforementioned negative correlation between performance and interpretability. To resolve this issue, we propose a method that can produce counterfactual maps from an already trained model. This post-hoc nature of our work not only provides a generalized framework that can be applied to most neural networks but also reduce the negative correlation since it can be applied to a model that already have high performance (*i.e.*, we can focus solely on interpretability with the higher performance given beforehand). Second, recent works on counterfactual explanation can only produce single [8, 12, 6] or dual [13, 32] sided explanation. In other words, they only consider one or two hypothetical scenarios for counterfactual reasoning (*e.g.*, producing maps that can only transform a numeric image to be classified as one or two specific numbers). With the help of a target attribution mechanism, our work, to the best of our knowledge, is the

first to propose *multi-way* counterfactual reasoning (*e.g.*, producing maps that can transform a numeric image to be classified as any other number).

To this end, we propose Born Identity Network (BIN<sup>1</sup>) that produces a counterfactual map using two components: The Counterfactual Map Generator, and the Target Attribution Network. The Counterfactual Map Generator is a variant of conditional GAN [22] that synthesizes a conditioned map, while the Target Attribution Network works in a complementary manner with Counterfactual Map Generator in enforcing a target counterfactual attribute to the synthesized conditioned map.

To evaluate our proposed framework, we perform a suite of analyses in various data domains: Numeric, geometric, and medical. First, to qualitatively test our work, we show and analyze the counterfactual maps for these above datasets. Second, to quantitatively validate the counterfactual map, we calculate a correlation measure between the counterfactual map and its ground truth map. Finally, we examine how each component of BIN works toward creating a counterfactual map with a suite of exhaustive ablation studies. The main contributions of our study are as follows<sup>2</sup>:

- We propose Born Identity Network (BIN), which, to the best of our knowledge, is the first work on producing counterfactual reasoning in *multiple* hypothetical scenarios.
- Our work produces a counterfactual map in a post-hoc manner, which can reduce the apparent negative correlation between performance and interpretability. This post-hoc nature makes our pro-

<sup>1</sup>We have coined this word to emphasize that the produced counterfactual map is a result of its original input, *i.e.*, its identity. Also, the post-hoc nature of our work fixes the weights, *i.e.*, the identity, of the deep learning model throughout the learning process.

<sup>2</sup>We released our Born Identity Network (BIN) codes on <https://anonymized.for.review>

posed network a generalized interpretation framework that can produce a counterfactual map from most pre-trained models.

## 2. Related Works

In this section, we describe various works proposed for explainable AI (XAI). First, we divide XAI into a general framework of attribution-based explanation and a more recent framework of counterfactual explanation.

### 2.1. Attribution-based Explanation

Attribution-based explanation refers to discovering or identifying the regions that have the most influence on deriving the outcome of a model. These approaches can further be divided into the gradient-based and reference-based explanation. First, the gradient-based explanation highlights the activation nodes that most contributed to the model’s decision. For example, Class Activate Map (CAM) [35], and Grad-CAM [26] highlights activation patterns of weights in a specified layer. In a similar manner, DeepTaylor [23], DeepLift [27], and Layer-wise Relevance Propagation (LRP) [1] highlight the gradients with regard to the prediction score. These approaches usually suffer from vanishing gradients due to the ReLU activation, and Integrated Gradients [30] resolves to solve this issue through sensitivity analysis. However, a crucial drawback of attribution-based approaches is that they tend to ignore features with relatively low discriminative power or highlight only those with overwhelming feature importance. Second, the reference-based explanation [34, 10, 6, 9] focuses on changes in model output with regards to perturbation in input samples. Various perturbation methods, such as masking [7], heuristic (*e.g.*, blurring, random noise) [6], region of the distractor image as reference for perturbation [13], or synthesized perturbation [9, 34, 10], has been proposed. One general drawback of these above attribution-based explanations is that they tend to produce low-resolution and blurred salient map. Our work can produce a crisp salient map with the same resolution as the input sample using a Generative Adversarial Network (GAN).

### 2.2. Counterfactual Explanations

Recently, more researchers have focused on counterfactual reasoning as a form of higher-level explanation. Counterfactual explanation refers to analyzing the model output with regards to hypothetical scenarios. For example, a counterfactual explanation could highlight those regions that may (hypothetically) cause a normal subject to be diagnosed with a disease. VAGAN [4] uses a variant of GAN that synthesizes a counterfactual map that transforms an input sample to be classified as an

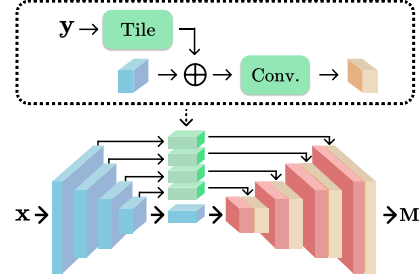


Figure 3. A detailed view of the generator. A tiled one-hot target label  $y$  is concatenated to the skip connection. This enables the generator to condition the counterfactual maps to be conditioned on an arbitrary target condition.

other label. However, VAGAN can only perform one-way synthesis (*e.g.*, the map that transforms input originally classified as A to be classified as B, but not vice versa), which limits the counterfactual explanation to also become single-sided. ICAM [2] was proposed as an extension to VAGAN to produce a dual-way counterfactual explanation. However, most real-world applications cannot be explained through single-/dual-sided explanation due to their complexity. Thus, our work proposes an approach for producing multi-way counterfactual explanation (*e.g.*, counterfactual map that can transform a numeric image to be classified as any other number).

## 3. Multi-way Counterfactual Map

Here, we formally define multi-way counterfactual map. First, we define a data set  $P = (P_x, P_y)$ , where  $(x, y) \sim P_{x,y}$  is the data, label pair and  $x \sim P_x, y \sim P_y$  is the unpaired data and label. We define a counterfactual map as a salient map that is able to produce a counterfactual explanation of a classifier  $\mathcal{E}$ . Formally, a single- or dual-way counterfactual map  $M_x$  is a map that when added to an input sample  $x$ , *i.e.*,  $\tilde{x} = x + M_x$ , the classifier classifies it as another label complement to its original label, *e.g.*,  $\mathcal{E}(x) = \text{true}$  and  $\mathcal{E}(\tilde{x}) = \text{false}$ , and vice versa for dual-way counterfactual map. Here, if we are able to condition this counterfactual map with an attribute (or label), *i.e.*,  $M_{x,y}$ , we are able to generate multi-way counterfactual map that transforms an input sample as any other attribute of interest:

$$\tilde{x} := x + M_{x,y} \quad \text{such that } \mathcal{E}(\tilde{x}) = y, \quad (1)$$

where data  $x$  and label  $y$  is unpaired, *i.e.*,  $x \sim P_x, y \sim P_y$ .

## 4. Born Identity Network

The goal of Born Identity Network (BIN) is to induce counterfactual reasoning dependent on the target condition from a pre-trained model. To achieve this

goal, we've devised BIN with two core modules, *i.e.*, Counterfactual Map Generator and Target Attribution Network, which work in a complementary manner in producing multi-way counterfactual map. Specifically, the Counterfactual Map Generator synthesizes a conditioned map, while the Target Attribution Network enforces a target attribution to the synthesized map (Figure 2.).

#### 4.1. Counterfactual Map Generator

The Counterfactual Map Generator is a variant of Conditional GAN [22] that can synthesize a counterfactual map conditioned on a target label  $\mathbf{y}$ , *i.e.*,  $\mathbf{M}_{\mathbf{x},\mathbf{y}}$ . Specifically, it consists of an encoder  $\mathcal{E}_\theta$ , a generator  $\mathcal{G}_\phi$ , and a discriminator  $\mathcal{D}_\psi$ . First, the network design of the encoder  $\mathcal{E}_\theta$  and the generator  $\mathcal{G}_\phi$  is a variation of U-Net [25] with tiled target label concatenated to the skip connections (Figure 3.). This generator design enables the generation to synthesize target conditioned maps such that multi-way counterfactual reasoning is possible. As a result, the counterfactual map is formulated as following:

$$\mathbf{M}_{\mathbf{x},\mathbf{y}} = \mathcal{G}_\phi(\mathcal{E}_\theta(\mathbf{x}), \mathbf{y}), \quad (2)$$

$$\tilde{\mathbf{x}} = \mathbf{x} + \mathbf{M}_{\mathbf{x},\mathbf{y}}. \quad (3)$$

Finally, following a general adversarial learning scheme, the discriminator discriminates real samples  $\hat{\mathbf{x}} \sim P_{\mathbf{x}}$  from synthesized samples  $\tilde{\mathbf{x}}$ .

Counterfactual reasoning requires a good balance between the proposed hypotheticals and given reality. In the following sections, we define the loss functions that guide the Counterfactual Map Generator to produce a well balanced counterfactual map.

##### 4.1.1 Adversarial Loss

For the adversarial loss functions, we have adopted the Least Square GAN (LSGAN) [21] objective function due to its stability during adversarial training. More specifically, LSGAN objective function contributes to a stable model training by penalizing samples far from the discriminator's decision boundary. This objective function is an important choice for BIN since the generated counterfactual maps should neither destroy the input sample nor ignore the target attribution, *i.e.*, it should contain a good balance between real and fake samples. To this end, the discriminator and the generator loss is defined as following, respectively:

$$\begin{aligned} \mathcal{L}_{adv}^{\mathcal{D}_\psi} &= \frac{1}{2} \mathbb{E}_{\hat{\mathbf{x}} \sim P_{\mathbf{x}}} [(D_\psi(\hat{\mathbf{x}}) - 1)^2] \\ &+ \frac{1}{2} \mathbb{E}_{\mathbf{x} \sim P_{\mathbf{x}}, \mathbf{y} \sim P_{\mathbf{y}}} [(D_\psi(\tilde{\mathbf{x}}))^2], \end{aligned} \quad (4)$$

$$\mathcal{L}_{adv}^{\mathcal{G}_\phi} = \frac{1}{2} \mathbb{E}_{\mathbf{x} \sim P_{\mathbf{x}}, \mathbf{y} \sim P_{\mathbf{y}}} [(D_\psi(\tilde{\mathbf{x}}) - 1)^2]. \quad (5)$$

#### 4.1.2 Cycle Consistency Loss

The cycle consistency loss is used for producing better *multi-way* counterfactual maps. Consider an one-way counterfactual map generator, where real samples  $\hat{\mathbf{x}}$  are always sampled from one specific class and synthesized samples  $\tilde{\mathbf{x}}$  from another. This setting does not require a cycle consistency loss since the real and fake samples always have specified labels. However, since our discriminator only classifies the real or fake samples, it does not have the ability to guide the generator to produce multi-way counterfactual maps. Thus, we add a cycle consistency loss where the forward cycle produces a map with an arbitrary condition, *i.e.*,  $\mathbf{M}_{\mathbf{x},\mathbf{y}}$  generated from an unpaired data  $\mathbf{x} \sim P_{\mathbf{x}}$  and label  $\mathbf{y} \sim P_{\mathbf{y}}$ , and the backward cycle produces a map conditioned on the input sample's label, *i.e.*,  $\mathbf{M}_{\tilde{\mathbf{x}},\mathbf{y}'}$  generated from paired data and label  $(\mathbf{x}, \mathbf{y}') \sim P_{\mathbf{x},\mathbf{y}}$ :

$$\mathcal{L}_{cyc} = \mathbb{E}_{(\mathbf{x}, \mathbf{y}') \sim P_{\mathbf{x},\mathbf{y}}, \mathbf{y} \sim P_{\mathbf{y}}} [\|(\tilde{\mathbf{x}} + \mathbf{M}_{\tilde{\mathbf{x}},\mathbf{y}'}) - \mathbf{x}\|_1], \quad (6)$$

where  $\mathbf{M}_{\tilde{\mathbf{x}},\mathbf{y}'} = \mathcal{G}_\phi(\mathcal{E}_\theta(\tilde{\mathbf{x}}), \mathbf{y}')$ .

#### 4.2. Target Attribution Network

The Target Attribution Network works in a complementary manner with the Counterfactual Map Generator in enforcing attribution to a synthesized counterfactual map. Specifically, the objective of the Target Attribution Network is to guide the generator to produce counterfactual maps that transform an input sample to be classified as a target class:

$$\mathcal{L}_{cls} = \mathbb{E}_{\mathbf{x} \sim P_{\mathbf{x}}, \mathbf{y} \sim P_{\mathbf{y}}} [CE(\mathbf{y}, \tilde{\mathbf{y}})], \quad (7)$$

where  $\mathbf{y}$  is the target label,  $\tilde{\mathbf{y}} = \mathcal{E}(\tilde{\mathbf{x}})$ , and  $CE$  is the cross entropy function.

Conceptually, the role of Target Attribution Network is similar to that of a discriminator in GANs, but their objective is very different. While a discriminator learns to distinguish between real and fake samples, the Target Attribution Network is already trained to classify the input samples. Thus, the discriminator plays a min-max game with a generator in an effort to produce more realistic samples, while the Target Attribution Network provides deterministic guidance for the generator to produce class-specific samples.

##### 4.2.1 Counterfactual Map Loss

The counterfactual map loss limits the values of the counterfactual map to grow:

$$\mathcal{L}_{map} = \mathbb{E}_{\mathbf{x} \sim P_{\mathbf{x}}, \mathbf{y} \sim P_{\mathbf{y}}} [\lambda_1 \|\mathbf{M}_{\mathbf{x},\mathbf{y}}\|_1 + \lambda_2 \|\mathbf{M}_{\mathbf{x},\mathbf{y}}\|_2], \quad (8)$$

where  $\lambda_1$  and  $\lambda_2$  are weighting constants. This loss is crucial in solving two issues in counterfactual map generation. First, when left untethered, the counterfactual

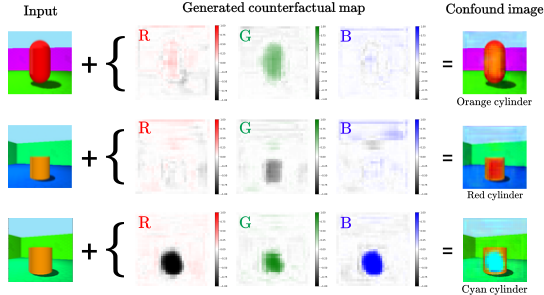


Figure 4. Examples of counterfactual maps for 3D Shapes [5] dataset. The counterfactual map consists of the RGB channel. Two models were trained separately for producing counterfactual maps for orange $\leftrightarrow$ red transformation and orange $\leftrightarrow$ cyan transformation.

map will destroy the identity of the input sample. This problem is related to adversarial attacks [33], where a simple perturbation to the input sample will change the model’s decision. Second, from an end-user point of view, only the most important features should be represented as the counterfactual explanation. Thus, by placing a constraint on the magnitude of counterfactual maps, we can address the above issues in one step.

### 4.3. Learning

Here, we define the overall loss function for BIN:

$$\mathcal{L} = \lambda_3 \mathcal{L}_{adv}^{\mathcal{D}_\psi} + \lambda_4 \mathcal{L}_{adv}^{\mathcal{G}_\phi} + \lambda_5 \mathcal{L}_{cyc} + \lambda_6 \mathcal{L}_{cls} + \mathcal{L}_{map}, \quad (9)$$

where  $\lambda$  is a weighting constant.

During training BIN, we have chosen to share and fix the weights of the encoder  $\mathcal{E}_\theta$  of Counterfactual Map Generator with the Target Attribution Network  $\mathcal{E}$  to ensure that the attribution is consistent throughout the generative process. However, preliminary experiments on training the encoder  $\mathcal{E}_\theta$  from scratch resulted in slightly lower qualitative and quantitative results.

## 5. Experiments

Here, we conduct various experiments to validate the counterfactual maps generated by our Born Identity Network (BIN). First, we conduct a qualitative analysis of dual- and multi-way counterfactual explanation. Second, we conduct a quantitative analysis using a correlation measure between generated counterfactual maps and ground-truth maps. Finally, we perform a suite of ablation studies to verify that each component of BIN towards creating a meaningful counterfactual map.

### 5.1. Datasets

For a comprehensive analysis of our work, we have chosen three data domains to perform our experiments. First, 3D Shapes dataset [5] is used for comparing dual-way counterfactual explanations. Second, MNIST [20]

is used for multi-way counterfactual explanations. Finally, ADNI (Alzheimer’s Disease Neuroimaging Initiative) [24] dataset is used as a real-world application in the medical domain.

**3D Shapes** The 3D Shapes dataset [5] consists of 480,000 RGB images of 3D geometric shapes with six latent factors (10 floors/wall/object hues, 8 scales, 4 shapes, and 15 orientations). For our experiments, we have chosen orange, red, cyan object hues as the target classes. Thus, although we use a total number of 144,000 images (48,000 per object hue), we only use images from two object hues for each experiment (*i.e.*, 96,000 images) since this dataset is intended for dual-way experiments. We have randomly split the dataset into a train, validation, and test sets at a ratio of 8:1:1 and applied channel-wise min-max normalization.

**MNIST** For MNIST dataset, we use the data split provided by [20] and applied min-max normalization.

**ADNI** ADNI dataset consists of 3D Magnetic Resonance Imaging (MRI) of various subject groups ranging from cognitive normal to Alzheimer’s disease. For this dataset, we have selected a baseline MRI of 425 Cognitive Normal (CN) subjects and 765 Alzheimer’s Disease (AD) subjects in ADNI 1/2/3/Go studies. Also, for longitudinal studies, we have selected 20 CN test subjects that have converted to the AD group in any given time. With the exception of 20 longitudinal test subjects, all subjects were randomly split into train, validation, and test sets at a ratio of 8:1:1. The pre-processing procedure consists of neck removal (FSL v6.0.1 robustfov), brain extraction (HDBet [17]), linear registration (FSL v6.0.1 FLIRT), zero-mean unit-variance normalization, quantile normalization at 5% and 95%, and down-scaling by 2 $\times$ . The resulting pre-processed MRI is a 96  $\times$  114  $\times$  96 image. We used default parameters from FSL v6.0.1 [18].

### 5.2. Implementation

We utilize an architecture of Kim *et al.* [19] for 3D Shapes dataset and minor modification of this network for MNIST. SonoNet-16 [3] is used for ADNI dataset as the encoder  $\mathcal{E}_\theta$  and the discriminator  $\mathcal{D}_\psi$ . The generator  $\mathcal{G}_\phi$  has the same network design as the encoder with pooling layers replaced by up-sampling layers. The test accuracy of the pre-trained Target Attribution Network  $\mathcal{E}$  is 99.56% for MNIST, 99.89% for 3D Shapes, 89.29% for ADNI dataset. Further details are in the Supplementary.

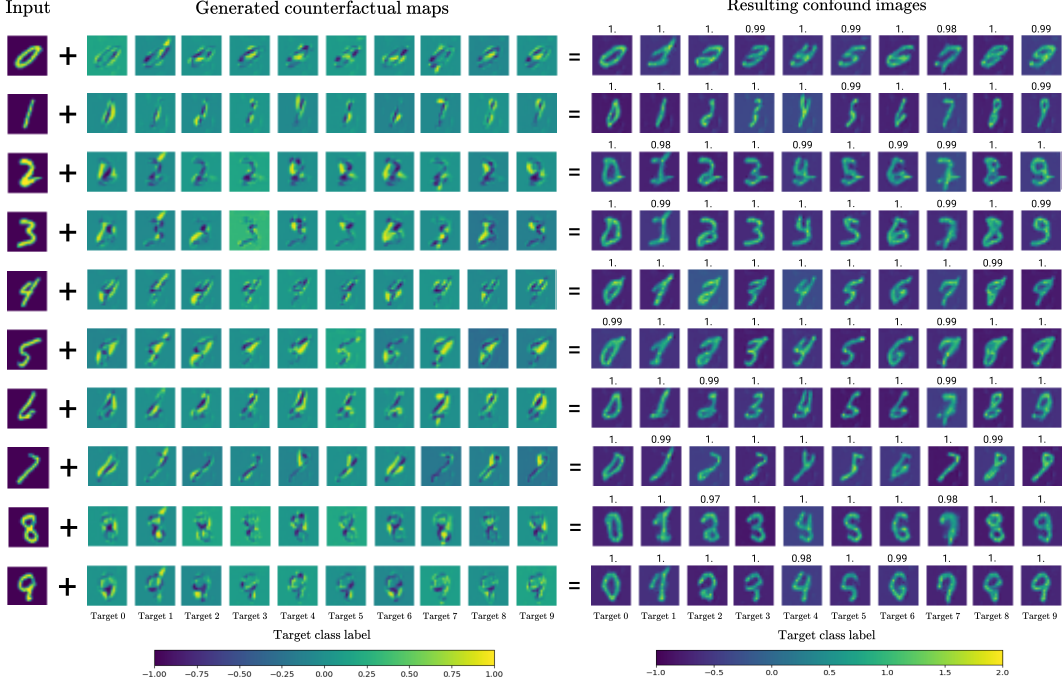


Figure 5. Examples of counterfactual maps for MNIST dataset. The resulting confound image is a addition between an input and its corresponding counterfactual map conditioned on a target label. The counterfactual maps maintains the style of the input samples while transforming them to target labels. The values on the top of each confound map is the model’s softmax activated logit.

Table 1. Fréchet Inception Distance (FID) scores reported for ablation studies for MNIST dataset.

y	Components			FID score									avg	
	$\mathcal{L}_{cls}$	$\mathcal{L}_{cyc}$	$\mathcal{L}_{map}$	0	1	2	3	4	5	6	7	8	9	
✓	✓	✓	✓	1.340	1.082	1.034	0.935	0.945	0.933	0.999	0.850	0.961	0.850	0.993
✓	✓	✓	✓	1.338	1.241	1.039	0.955	1.064	0.973	1.022	0.956	0.993	0.935	1.052
✓	✓	✓	✓	1.283	1.156	0.915	0.810	0.959	0.822	0.987	0.888	0.896	0.834	0.955
✓	✓	✓	✓	1.318	1.056	0.906	0.804	0.951	0.824	1.001	0.841	0.904	0.841	0.945
✓			✓	1.338	1.242	1.039	0.956	1.065	0.973	1.022	0.956	0.993	0.935	1.052
				1.338	1.242	1.039	0.956	1.065	0.973	1.022	0.956	0.993	0.935	1.052
✓	✓	✓	✓	<b>1.211</b>	<b>0.902</b>	<b>0.892</b>	<b>0.802</b>	0.958	<b>0.812</b>	<b>0.970</b>	<b>0.835</b>	0.912	<b>0.833</b>	<b>0.912</b>

Table 2. NCC scores for 3D Shapes and ADNI dataset.

Method	3D Shapes		ADNI	
	NCC(+)	NCC(-)	NCC(+)	NCC(-)
LRP-Z [1]	0.008	0.086	0.004	0.005
Integrated Gradients [30]	0.006	0.152	0.006	0.004
DeepLIFT [27]	0.007	0.183	0.005	0.003
Guided Backprop [26]	0.183	0.123	0.225	<b>0.198</b>
VA-GAN [4]	0.381	-	0.282	-
<b>BIN</b>	<b>0.516</b>	<b>0.465</b>	<b>0.306</b>	0.185

Table 3. NCC scores for ablation studies.

Removed	3D Shapes		ADNI	
	NCC(+)	NCC(-)	NCC(+)	NCC(-)
<b>y</b>	0.271	0.259	0.211	0.088
$\mathcal{L}_{cls}$	0.199	0.126	0.065	0.063
$\mathcal{L}_{cyc}$	0.482	0.336	0.253	0.125
$\mathcal{L}_{map}$	0.238	0.159	0.248	0.158
$\mathcal{L}_{cls}, \mathcal{L}_{map}$	0.089	0.068	0.088	0.082
All above	0.033	0.064	0.076	0.053
<b>BIN</b>	<b>0.516</b>	<b>0.465</b>	<b>0.306</b>	<b>0.185</b>

### 5.3. Qualitative Analysis

An  $N$ -way counterfactual map is a map that when added to an input sample, the classifier classifies it as a targeted class. The  $N$ -way term refers to the degree of freedom of the targeted class. For example, a dual-way counterfactual map can transform a red cylinder to be classified as an orange or an orange cylinder to be classified as a red (Figure 4.). In the following sections, we compare and validate multi-way counterfactual maps in various settings. Specifically, we take a bottom-up analysis approach with experiments on a toy example building up to application in a real-world dataset. First, we analyze the dual-way counterfactual maps with a toy example of 3D Shapes dataset. Then, we validate our novel multi-way counterfactual maps with MNIST dataset. Finally, we apply our proposed BIN in a real-world dataset and compare it with state-of-the-art XAI frameworks with ADNI dataset.

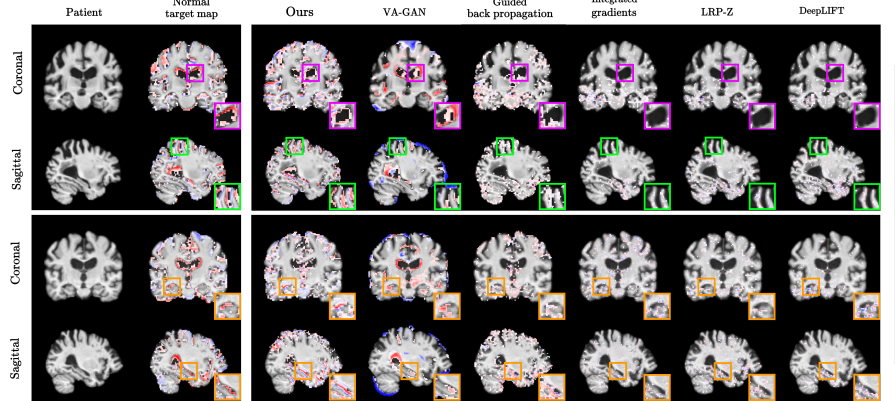


Figure 6. Example of counterfactual maps for ADNI dataset. Purple box visualize ventricular regions (top row), green box visualize cortex regions (second row), and orange box visual hippocampal regions (bottom two rows). (VA-GAN, Guided back-propagation, Integrated gradients, LRP-Z, DeepLift)

### 5.3.1 Validation of Counterfactual Map

First, we analyze dual-way counterfactual maps using a toy example of 3D Shapes dataset (Figure 4.). The goal of this experiment is to verify that our counterfactual map is able to transform an input image with regard to the target latent factor, *i.e.*, object hue. The first and second row shows a counterfactual map for transforming red (R: 255, G: 0, B: 0) to orange (R: 255, G: 150, B: 0), and orange to red. Transforming red to orange is a relatively simpler task since it only requires a transformation in the G channel. As a result, R and B channels of our counterfactual maps are highlighted relatively less than the G channel. The third row transforms orange (R: 255, G: 150, B: 0) to cyan (R: 0, G: 210, B: 255). Despite the contrasting color in all channels, BIN is able to induce the counterfactual map corresponding to the target object hue. In addition, the classification performance on the synthesized image is 99.51%, indicating that the counterfactual map has successfully transformed the input image to be classified as another label.

In most counterfactual maps generated in this experiment, we have observed an interesting phenomenon in which the counterfactual maps are relatively *invariant* to latent factors that were not targeted for transformation. For example, the scale and shape of the object in the counterfactual map are relatively similar to that of the input image. This indicates that our counterfactual map is somewhat localized to the target latent factor.

### 5.3.2 Invariant of Counterfactual Map

For this experiment, we generate multi-way counterfactual maps for MNIST dataset (Figure 5.). In plain sight, we can observe that the style of an input image is maintained. For example, with confound images of 1 (second row), which are one of the least realistic confound

images, we can observe that the transformation maintains the style of the input image. This is related to the invariant to non-targeted latent factors observed in section 5.3.1. We hypothesize that this invariant is due to the counterfactual map loss (eq. (8)) since it puts constraints on the values of the counterfactual map so that it transforms an input sample with the least amount of energy. From a conceptual view, our generated counterfactual map is a good example of counterfactual reasoning since it can successfully produce hypothetical realities with regards to a given input sample.

### 5.3.3 Application in Medical Domain

The first part of this section compares BIN with various XAI frameworks (Figure 6.). Since there are no ground truth maps for ADNI dataset, we utilize the Normal target map from longitudinal test subjects. First, we have gathered MRI from subjects that were originally a part of CN group but converted to AD group in any given time. Then, we subtracted the baseline image from the image at the time of AD conversion to create the Normal target map. This Normal target map is a good representation of a ground truth map of disease localization since we can observe which regions are possibly responsible for AD conversion. For attribution-based approaches (Integrated gradients [30], LRP-Z [1], DeepLift [27]) and perturbation-based approach (Guided backpropagation [26]), we use the pre-trained Target Attribution Network  $\mathcal{E}$  as the classifier.

One of the biomarkers of Alzheimer’s disease is the atrophy in brain regions, such as the ventricular, cortical thickness, and hippocampus [16]. As observed in the Normal target map (second column in Figure 6), atrophy is clearly visible in those regions. The counterfactual map generated by attribution-based approaches (Integrated gradients, LRP-Z, DeepLift) and perturbation-

based approach (Guided backpropagation) do not clearly show the regions responsible for. Also, comparing our proposed BIN with VA-GAN, our work clearly shows a better representation of the Normal target map. In an extension to the above experiment, we have performed an interpolation between AD and CN by conditioning the counterfactual map with interpolated target classes (in the Supplementary).

#### 5.4. Quantitative Analysis

In this section, we quantitatively evaluate our proposed BIN and compare the outcomes. To quantitatively assess the quality of our generated counterfactual maps, we've calculated the Normalized Cross Correlation (NCC) score between the generated maps and the ground-truth maps. NCC score measures the similarity between two samples in a normalized setting. Thus, NCC can be helpful when two samples have a different magnitude of signals. However, since MNIST dataset does not have ground truth maps, we have performed a different quantitative evaluation in section 5.5. For the ADNI dataset, we use the Normal target map described in section 5.3.3 as the ground truth map. NCC(+) refers to the counterfactual map for transforming red cylinder to orange cylinder for 3D Shapes, and AD to CN for ADNI dataset (vice versa for NCC(-)). Higher NCC scores denote higher similarity (*i.e.*, better performance).

In Table 2, we report NCC scores for 3D Shapes and ADNI dataset. Attribution-based methods (LRP-Z, Integrated gradients, and DeepLift) tend to have lower scores since lower discriminative features can be ignored in domains with high complexity, which is evident in Figure 6. Counterfactual maps for VA-GAN can only transform input from AD to CN, thus NCC(-) scores cannot be calculated. Our proposed BIN has a outstanding NCC(+) scores indicating that the addition operation is a stronger suit than the subtraction operation. A further discussion on why NCC(-) is lower in section 6.

#### 5.5. Ablation Studies

In this section, we perform a suite of ablation studies to assess each component of BIN in creating a counterfactual map. Specifically, we perform ablation studies on the conditioned generator (denoted as  $y$ ), the Target Attribution Network loss ( $\mathcal{L}_{cls}$ ), cycle consistency loss ( $\mathcal{L}_{cyc}$ ), and the Counterfactual Map loss ( $\mathcal{L}_{map}$ ).

**Normalized Cross Correlation** For the ADNI and 3D Shapes dataset, we calculate the Normalized Cross Correlation (NCC) score with the same settings as section 5.4 (Table 3). The reported scores indicate every

component of BIN is crucial for producing a meaningful counterfactual map. However, ablating the Target Attribution Network loss  $\mathcal{L}_{cls}$  shows a significant drop in NCC scores, indicating that it is one of the most crucial component of BIN. The Target Attribution Network guides the generative process to build targeted class attribution, which works in a similar manner to a discriminator in GANs. The cycle consistency loss  $\mathcal{L}_{cyc}$  ensures the counterfactual map to contain information on its identity, *i.e.*, input sample. In a preliminary experiment, we have observed that cycle consistency loss help generate more crisp counterfactual maps, indicating that it works as a regularizer for BIN. The counterfactual map loss  $\mathcal{L}_{map}$  is another important component of the BIN since it regulates which region is most important.

**Fréchet Inception Distance** For a quantitative assessment of multi-way counterfactual map, we use a Fréchet Inception Distance [14] commonly used for assessing the generative performance of GANs. Here, we've selected 4,000 test samples for counterfactual map generation (*i.e.* fake images), and 4,000 test samples as real images. Since a counterfactual map can transform any number to any other number, a single image can generate 10 images (one per number). Thus, the total number of fake samples we've generated is 40,000 (*i.e.*, 4,000 fake images per number). To best of our knowledge, our proposed BIN is the first to perform multi-way counterfactual map generation. Thus, we compare our work in an ablation study setting (Table 1). In most of the settings, our proposed BIN performs significantly better.

### 6. Discussion

For most experiments, reported NCC(-) scores for almost every compared method were lower than that of NCC(+). A possible explanation is that the activation functions, such as ReLU, may be imposing a positive bias or negative skewness on the model output. For example, the mean and mode of a counterfactual map for almost every datasets and every method compared in this paper were slightly over zero. This may result in imposing a constraint for subtraction operations which lowers the NCC(-) scores. Possible future work for the community is to verify whether this bias or skewness really exists and propose a way to alleviate this.

### 7. Conclusion

In this work, we propose Born Identity Network (BIN), which is a post-hoc approach for producing multi-way counterfactual map. We demonstrate that our method can be easily applied to various networks. Fidelity of performance is secured by visualizing a causal

relationship for prediction. That is, we show that counterfactual maps can provide end-users with an intuitive explanation of classification results.

**Acknowledge** This work was supported by the Institute of Information & Communications Technology Planning & Evaluation (IITP) grant funded by the Korea Government (MSIT) (No. 2017-0-01779, A machine learning and statistical inference framework for explainable artificial intelligence). This work was also supported by the Institute of Information & Communications Technology Planning & Evaluation (IITP) grant funded by the Korea Government (MSIT) (No. 2019-0-00079, Department of Artificial Intelligence (Korea University)).

## References

- [1] Sebastian Bach, Alexander Binder, Grégoire Montavon, Frederick Klauschen, Klaus-Robert Müller, and Wojciech Samek. On pixel-wise explanations for non-linear classifier decisions by layer-wise relevance propagation. *Public Library of Science ONE*, 10(7):e0130140, 2015.
- [2] Cher Bass, Mariana da Silva, Carole Sudre, Petru-Daniel Tudosiu, Stephen Smith, and Emma Robinson. Icam: Interpretable classification via disentangled representations and feature attribution mapping. In *Advances in Neural Information Processing Systems*, volume 33, 2020.
- [3] Christian F Baumgartner, Konstantinos Kamnitsas, Jacqueline Matthew, Tara P Fletcher, Sandra Smith, Lisa M Koch, Bernhard Kainz, and Daniel Rueckert. Sononet: Real-time detection and localisation of fetal standard scan planes in freehand ultrasound. *IEEE Transactions on Medical Imaging*, 36(11):2204–2215, 2017.
- [4] Christian F Baumgartner, Lisa M Koch, Kerem Can Tezcan, Jia Xi Ang, and Ender Konukoglu. Visual feature attribution using wasserstein gans. In *Proceedings of the IEEE Conference on Computer Vision and Pattern Recognition*, pages 8309–8319, 2018.
- [5] Chris Burgess and Hyunjik Kim. 3d shapes dataset. <https://github.com/deepmind/3dshapes-dataset/>, 2018.
- [6] Chun-Hao Chang, Elliot Creager, Anna Goldenberg, and David Duvenaud. Explaining image classifiers by counterfactual generation. *arXiv preprint arXiv:1807.08024*, 2018.
- [7] Piotr Dabkowski and Yarin Gal. Real time image saliency for black box classifiers. In *Advances in Neural Information Processing Systems*, pages 6967–6976, 2017.
- [8] Saloni Dash and Amit Sharma. Counterfactual generation and fairness evaluation using adversarially learned inference. *arXiv preprint arXiv:2009.08270*, 2020.
- [9] Amit Dhurandhar, Pin-Yu Chen, Ronny Luss, Chun-Chen Tu, Paishun Ting, Karthikeyan Shanmugam, and Payel Das. Explanations based on the missing: Towards contrastive explanations with pertinent negatives. In *Advances in Neural Information Processing Systems*, pages 592–603, 2018.
- [10] Ruth C Fong and Andrea Vedaldi. Interpretable explanations of black boxes by meaningful perturbation. In *Proceedings of the IEEE International Conference on Computer Vision*, pages 3429–3437, 2017.
- [11] Leilani H Gilpin, David Bau, Ben Z Yuan, Ayesha Bajwa, Michael Specter, and Lalana Kagal. Explaining explanations: An overview of interpretability of machine learning. In *Proceedings of the International Conference on Data Science and Advanced Analytics*, pages 80–89. IEEE, 2018.
- [12] Yash Goyal, Amir Feder, Uri Shalit, and Been Kim. Explaining classifiers with causal concept effect (cace). *arXiv preprint arXiv:1907.07165*, 2019.
- [13] Yash Goyal, Ziyan Wu, Jan Ernst, Dhruv Batra, Devi Parikh, and Stefan Lee. Counterfactual visual explanations. *arXiv preprint arXiv:1904.07451*, 2019.
- [14] Martin Heusel, Hubert Ramsauer, Thomas Unterthiner, Bernhard Nessler, and Sepp Hochreiter. Gans trained by a two time-scale update rule converge to a local nash equilibrium. In *Advances in neural information processing systems*, pages 6626–6637, 2017.
- [15] Sara Hooker, Dumitru Erhan, Pieter-Jan Kindermans, and Been Kim. A benchmark for interpretability methods in deep neural networks. In *Advances in Neural Information Processing Systems*, pages 9737–9748, 2019.
- [16] Khalid Iqbal, Michael Flory, Sabiha Khatoon, Hilkka Soininen, Tuula Pirttila, Maarit Lehtovirta, Irina Alafuzoff, Kaj Blennow, Niels Andreasen, Eugeen Vanmechelen, et al. Subgroups of alzheimer’s disease based on cerebrospinal fluid molecular markers. *Annals of Neurology: Official Journal of the American Neurological Association and the Child Neurology Society*, 58(5):748–757, 2005.
- [17] Fabian Isensee, Marianne Schell, Irada Pflueger, Gianluca Brugnara, David Bonekamp, Ulf Neuberger, Antje Wick, Heinz-Peter Schlemmer, Sabine Heiland, Wolfgang Wick, Martin Bendszus, Klaus H. Maier-Hein, and Philipp Kickingereder. Automated brain extraction of multisequence mri using artificial neural networks. *Human Brain Mapping*, 40(17):4952–4964, 2019.
- [18] Mark Jenkinson, Christian F. Beckmann, Timothy E.J. Behrens, Mark W. Woolrich, and Stephen M. Smith. Fsl. *NeuroImage*, 62(2):782 – 790, 2012. 20 YEARS OF fMRI.
- [19] Hyunjik Kim and Andriy Mnih. Disentangling by factorising. *arXiv preprint arXiv:1802.05983*, 2018.
- [20] Yann LeCun. The mnist database of handwritten digits. <http://yann.lecun.com/exdb/mnist/>, 1998.
- [21] Xudong Mao, Qing Li, Haoran Xie, Raymond YK Lau, Zhen Wang, and Stephen Paul Smolley. Least squares generative adversarial networks. In *Proceedings of the IEEE International Conference on Computer Vision*, pages 2794–2802, 2017.
- [22] Mehdi Mirza and Simon Osindero. Conditional generative adversarial nets. *arXiv preprint arXiv:1411.1784*, 2014.
- [23] Grégoire Montavon, Sebastian Lapuschkin, Alexander Binder, Wojciech Samek, and Klaus-Robert Müller. Ex-

plaining nonlinear classification decisions with deep taylor decomposition. *Pattern Recognition*, 65:211–222, 2017.

- [24] Susanne G. Mueller, Michael W. Weiner, Leon J. Thal, Ronald C. Petersen, Clifford Jack, William Jagust, John Q. Trojanowski, Arthur W. Toga, and Laurel Beckett. The alzheimer’s disease neuroimaging initiative. *Neuroimaging Clinics of North America*, 15(4):869 – 877, 2005. Alzheimer’s Disease: 100 Years of Progress.
- [25] Olaf Ronneberger, Philipp Fischer, and Thomas Brox. U-net: Convolutional networks for biomedical image segmentation. In *Proceedings of the International Conference on Medical Image Computing and Computer-Assisted Intervention*, pages 234–241. Springer, 2015.
- [26] Ramprasaath R Selvaraju, Michael Cogswell, Abhishek Das, Ramakrishna Vedantam, Devi Parikh, and Dhruv Batra. Grad-cam: Visual explanations from deep networks via gradient-based localization. In *Proceedings of the IEEE International Conference on Computer Vision*, pages 618–626, 2017.
- [27] Avanti Shrikumar, Peyton Greenside, and Anshul Kundaje. Learning important features through propagating activation differences. *arXiv preprint arXiv:1704.02685*, 2017.
- [28] Karen Simonyan, Andrea Vedaldi, and Andrew Zisserman. Deep inside convolutional networks: Visualising image classification models and saliency maps. *arXiv preprint arXiv:1312.6034*, 2013.
- [29] Daniel Smilkov, Nikhil Thorat, Been Kim, Fernanda Viégas, and Martin Wattenberg. Smoothgrad: Removing noise by adding noise. *arXiv preprint arXiv:1706.03825*, 2017.
- [30] Mukund Sundararajan, Ankur Taly, and Qiqi Yan. Axiomatic attribution for deep networks. *arXiv preprint arXiv:1703.01365*, 2017.
- [31] Arnaud Van Looveren and Janis Klaise. Interpretable counterfactual explanations guided by prototypes. *arXiv preprint arXiv:1907.02584*, 2019.
- [32] Pei Wang and Nuno Vasconcelos. Scout: Self-aware discriminant counterfactual explanations. In *Proceedings of the IEEE Conference on Computer Vision and Pattern Recognition*, June 2020.
- [33] Kaidi Xu, Sijia Liu, Pu Zhao, Pin-Yu Chen, Huan Zhang, Quanfu Fan, Deniz Erdogmus, Yanzhi Wang, and Xue Lin. Structured adversarial attack: Towards general implementation and better interpretability. *arXiv preprint arXiv:1808.01664*, 2018.
- [34] Matthew D Zeiler and Rob Fergus. Visualizing and understanding convolutional networks. In *Proceedings of the European Conference on Computer Vision*, pages 818–833. Springer, 2014.
- [35] Bolei Zhou, Aditya Khosla, Agata Lapedriza, Aude Oliva, and Antonio Torralba. Learning deep features for discriminative localization. In *Proceedings of the IEEE Conference on Computer Vision and Pattern Recognition*, pages 2921–2929, 2016.